One-dimensional photonic crystals bound by light

Liyong Cui,[1] Xiao Li,[1] Jun Chen,[2] Yongyin Cao,[3] Guiqiang Du,[4] and Jack Ng[1,5,*]

[1]*Department of Physics, Hong Kong Baptist University, Hong Kong, China*

[2]*Institute of Theoretical Physics and Collaborative Innovation Center of Extreme Optics, Shanxi University, Shanxi, China*

[3]*Department of Physics, Harbin Institute of Technology, Harbin, 150001, China*

[4]*School of Space Science and Physics, Shandong University at Weihai, Weihai, 264209, China*

[5]*Institute of Computational and Theoretical Studies, Hong Kong Baptist University, Kowloon Tong, Hong Kong, China*

(Received 5 June 2017; published 14 August 2017)

Through rigorous simulations, the light scattering induced optical binding of one-dimensional (1D) dielectric photonic crystals is studied. The optical forces corresponding to the pass band, band gap, and band edge are qualitatively different. It is shown that light can induce self-organization of dielectric slabs into stable photonic crystals, with its lower band edge coinciding with the incident light frequency. Incident light at normal and oblique incidence and photonic crystals with parity-time symmetry are also considered.

DOI: 10.1103/PhysRevA.96.023833

I. INTRODUCTION

Optical trapping—the localization and manipulation of small particles by a carefully sculpted laser beam—has become an invaluable tool in various scientific areas spanning fundamental and applied sciences [1–7], wherever small particles are involved. Ingenious ways were invented to shape the laser beam to achieve novel functionalities. Nevertheless, the simultaneous manipulation of a collection of particles in proximity is still rather challenging: The particles scatter light, thereby redistributing the spatial light intensity, which in turn alters the optical force [8–10]. In other words, the optical forces are not solely determined by the incident field, but also by the distribution of the particles. Such mutual interaction is termed "optical binding" [8] and has been investigated experimentally [11–19] and theoretically [20–29].

This paper is devoted to the optical binding in one-dimensional (1D) dielectric photonic crystals (PCs), which consist of periodically arranged dielectric slabs in air. By using the transfer matrix method [30], we calculated the electromagnetic fields within a 1D PC consisting of N dielectric slabs, where N ranges from 20 to 1000 in our calculation. We then calculated the time-averaged optical force using a surface integral of the Maxwell stress tensor. We then searched for equilibrium configurations of the PC by using molecular static simulation [31]. Finally, we verified the stability of the PC in equilibrium using the linear stability analysis.

We rigorously showed that a 1D PC consisting of alternating dielectric and air layers can be stabilized by illuminating it with a laser tuned to the lower band edge of the PC. The dynamical matrix approach was also employed to verify the stability of a PC with infinitely many unit cells. We considered a 1D PC at normal or oblique incidence.

Last but not least, we studied a 1D PC with parity-time ($\mathcal{PT}$) symmetry, where the dielectric constant now satisfies $\varepsilon(x) = \varepsilon^*(-x)$. The Hermiticity of an operator for a physically observable quantity is a fundamental axiom in quantum mechanics, which guarantees a real eigenvalues spectrum. Bender *et al.* showed that a $\mathcal{PT}$-symmetric Hamiltonian can also guarantee a real spectrum. It has been shown that an optical system can also possess $\mathcal{PT}$ symmetry [32]. Here we showed that when the $\mathcal{PT}$ symmetry is exact, the optical binding of a 1D PC could also organize itself into a stable PC.

II. RESULTS

A. Optical forces in a 1D dielectric PC

We consider an N-slab PC consisting of alternating dielectric and air layers. Its unit cell is illustrated in Fig. 1(a). The corresponding photonic band structure calculated by the standard transfer matrix method [30] is plotted in Fig. 1(b), where $\varepsilon_{\text{diel}} = 4$ (dielectric constant of the dielectric), $\mu_{\text{diel}} = 1$ (permeability of the dielectric), $d_{\text{diel}} = 80\,\text{nm}$ (thickness of the dielectric), and $d_{\text{air}} = 120\,\text{nm}$ (thickness of air). The same physics was observed when similar dielectric constants and lattice constants were used.

Under laser illumination, light can exert optical forces on the slabs. For the collection of parallel, infinitely large dielectric slabs in air, the time-averaged optical force $\mathbf{F}$ (hereafter referred to as the "optical force" for simplicity) is given by

$$\mathbf{F} = \sum_{i=1}^{6} \int_{\text{surface } i} \overleftrightarrow{\mathbf{T}} \cdot d\mathbf{a} = \int_{\text{surface 1}} \overleftrightarrow{\mathbf{T}} \cdot d\mathbf{a} + \int_{\text{surface 2}} \overleftrightarrow{\mathbf{T}} \cdot d\mathbf{a}, \tag{1}$$

where $\mathbf{a}$ is the area of the surface, the surfaces 1–4 are depicted in Fig. 1(a) by the yellow dotted lines, and the surfaces 5 and 6 are the top and bottom cover of the rectangle formed by surfaces 1–4. The time-averaged Maxwell stress tensor in the air (surfaces 1 and 2) [33] is given by

$$\overleftrightarrow{\mathbf{T}} = \frac{1}{2}\varepsilon_0 \left[\mathbf{E}\mathbf{E}^* + c^2 \mathbf{B}\mathbf{B}^* - \frac{1}{2}(\mathbf{E}\cdot\mathbf{E}^*)\overleftrightarrow{\mathbf{I}} - \frac{c^2}{2}(\mathbf{B}\cdot\mathbf{B}^*)\overleftrightarrow{\mathbf{I}} \right], \tag{2}$$

where $\mathbf{E}$ and $\mathbf{B}$ are the electric and magnetic fields, ε_0 is the permittivity of the free space, c is the light speed in vacuum, $\overleftrightarrow{\mathbf{I}}$ is the 3×3 identity matrix, and * denotes taking the complex conjugate. By symmetry, the contributions from surfaces 3 and 4, and 5 and 6 (which are not shown) are canceled. For TE and

*jacktfng@hkbu.edu.hk

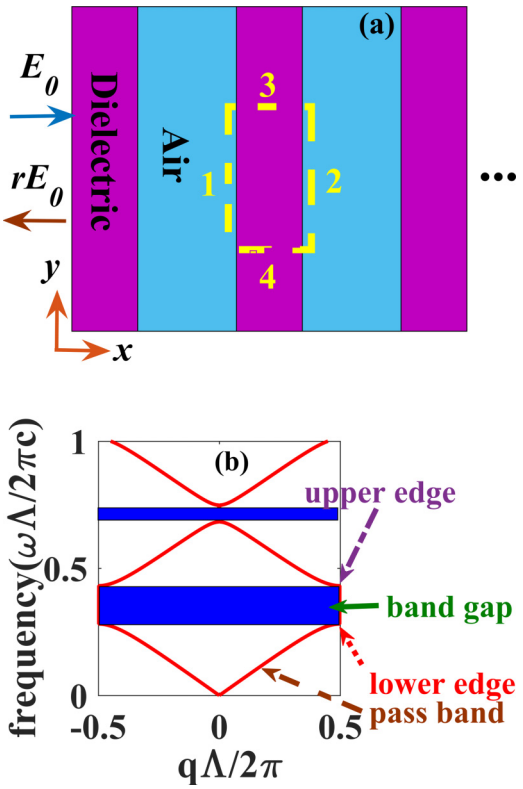

FIG. 1. (a) Schematic showing a linearly polarized plane wave with a modest intensity of 1.33×10^{-2} mW/μm^2 normally incident on a PC consisting of alternating layer of dielectrics and air. (b) The photonic band structure for a PC with $\varepsilon_{\text{diel}} = 4$, $\varepsilon_{\text{air}} = 1$, $\mu_{\text{diel}} = \mu_{\text{air}} = 1$, $d_{\text{diel}} = 80$ nm, and $d_{\text{air}} = 120$ nm. Here q is the Bloch wave vector and $\Lambda = d_{\text{diel}} + d_{\text{air}}$. The photonic band gap is shaded in blue.

TM incidence, Eq. (1) can be simplified to

$$\frac{F_z}{A} = \frac{1}{2}\varepsilon_0(|A_0|^2 + |B_0|^2 - |C_0|^2 - |D_0|^2)\cos^2\theta. \quad (3)$$

Here F_z/A is the z component of optical force per unit area, θ is the incident angle, $|A_0|$ and $|B_0|$ are the amplitudes of the forward and backward electric field on the left side of the slab (surface 1), and $|C_0|$ and $|D_0|$ are the corresponding quantities on the right side (surface 2).

Figures 2 and 3 plot the optical forces acting on the PC when it was illuminated at the four selected frequencies marked by the arrows in Fig. 1(b) at normal incidence. When illuminated at the pass band [Fig. 2(a)], the optical forces oscillate along the length of the PC, due to the interference between the forward and backward propagating waves. We note that since the reflected waves for the PC with 20 and 40 slabs are different, their optical forces are also different. However, the oscillatory character of the optical force is generic for PCs illuminated at a frequency within the pass band. It is noteworthy that the amplitude of oscillating force vanishes when $2\sqrt{\varepsilon_{\text{diel}}}d_{\text{diel}} = m\lambda\,(m = 1,2,3\cdots)$, where λ is the incident wavelength in air. This condition corresponds to unit transmission for every slab and thus the force goes to zero. The forces associated with an incident wavelength inside the first band gap were plotted in Figs. 2(b) and 3(b). The field attenuates rapidly as it propagates through the PC, so are the

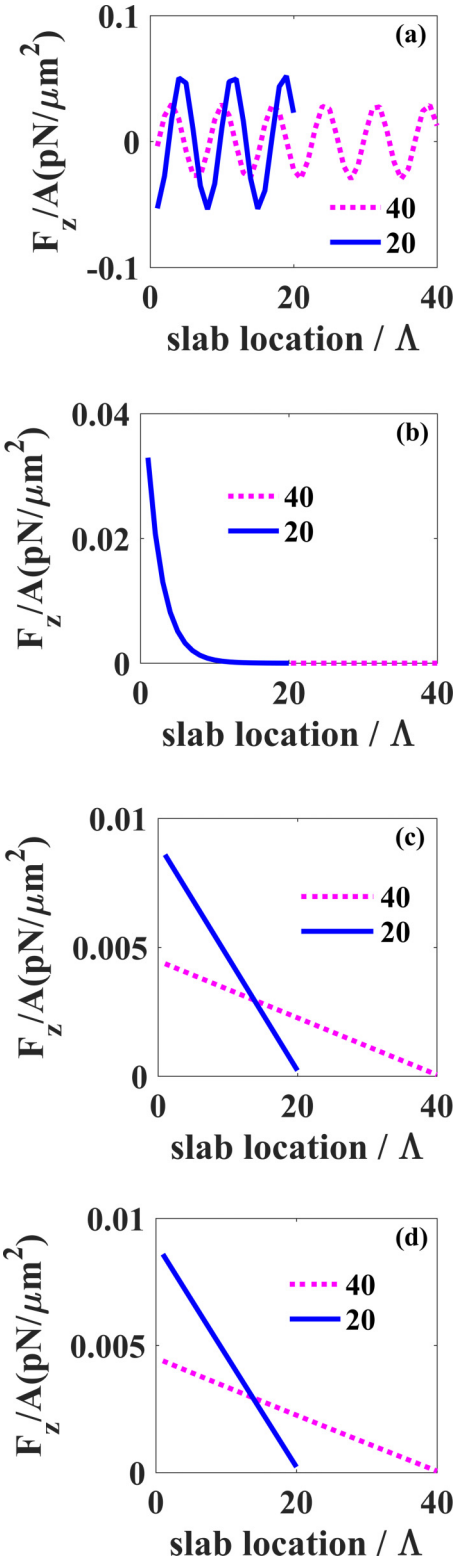

FIG. 2. The optical forces acting on the individual slab at the four representative frequencies marked in Fig. 1(b) by colored arrows. Solid blue line: 20 slabs; dotted magenta line: 40 slabs. (a) Pass band marked by the dashed-dotted orange arrow, (b) band gap marked by the solid green arrow, (c) lower band edge marked by the dotted red arrow, and (d) upper band edge marked by the dashed violet arrow.

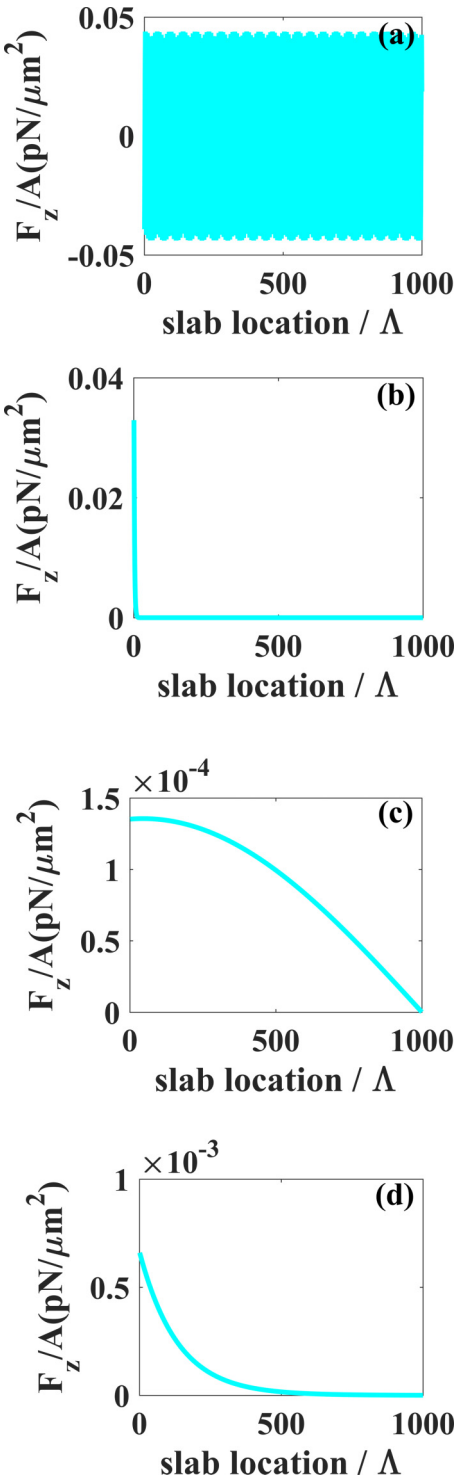

FIG. 3. The optical forces acting on an $N = 1000$ PC at the four representative frequencies marked by arrows in Fig. 1(b). (a) Pass band marked by the dashed-dotted orange arrow, (b) band gap marked by the solid green arrow, (c) lower band edge marked by the dotted red arrow, and (d) upper band edge marked by the dashed violet arrow.

forces. Figures 2(c) and 3(c) show the forces associated with the lower band edges while Figs. 2(d) and 3(d) show the forces associated with the upper band edges. The curves in Figs. 2(c) and 2(d) appear to be linear, but for a larger PC, as shown in Figs. 3(c) and 3(d), the linear relationship no longer holds.

B. Equilibrium configurations

As discussed in Sec. II A and depicted in Fig. 2, the force acting on a PC is generally nonzero. We shall now explore the possibility of binding and self-organizing a 1D PC using light induced forces. We searched for equilibrium configurations where the force acting on each slab is zero or equal using molecular static simulations [31] by relaxing a periodic PC. The former is known as static equilibrium (zero force), while the latter is known as dynamical equilibrium (equal force) where the entire structure will move with its shape being fixed.

The simulation results can be summarized as follows. After relaxation, if an equilibrium configuration is found, the slabs sometimes organize themselves into aperiodic structures (especially for small N), sometimes a PC with a nearly uniform separation between the slabs (for large N). Irrespective of the incident wavelength, the equilibriums found (if any) using molecular static are dynamic equilibrium configurations. When the reflection of light is not zero, the total force acting on the entire PC has to be greater than zero. Accordingly, dynamic equilibrium is the only possibility, as static equilibrium must have zero total force. Moreover, dynamical equilibrium with more slabs will generally be associated with a smaller force on each slab, as $F_z/A \sim 1/N$ for each slab (the values of the force per unit area on each slab for dynamic equilibrium with $N = 50$, 500, and 1000 are, respectively, 3.5×10^{-3}, 3.6×10^{-4}, and 1.8×10^{-4} in units of pN/μm^2 at an incident light intensity of 1.33×10^{-2} mW/μm^2). The equilibrium separations (lattice constants) between adjacent slabs were plotted in Fig. 4. The lattice constant is generally uniform except near the end of the PC. We also identified the corresponding static equilibriums when the PC is illuminated by a pair of identical counterpropagating plane waves, either coherent or incoherent, as shown in Fig. 5. The lattice constants are shown in Fig. 5(a) and 5(b) for coherent and incoherent counterpropagating waves, which are highly uniform.

Figure 6 plotted the band structure for a PC before (solid blue line) and after (dashed red line) relaxation. The initial PC was being illuminated by a linear polarized plane wave at the upper band edge of its first band gap. After relaxation, the PC rearranged itself into another PC whose lower band edge coincided with the incident light frequency. This same

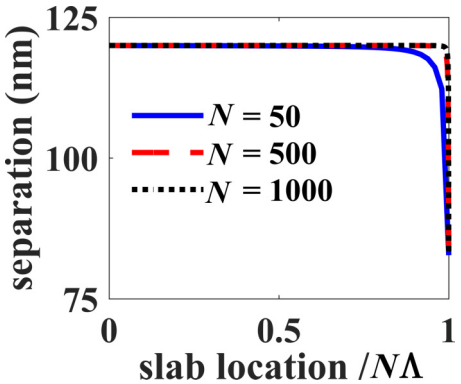

FIG. 4. The separations (or lattice constants) between two adjacent slabs in stable PCs with 50 (solid blue line), 500 (dashed red line), and 1000 (dotted black line) slabs bound by light.

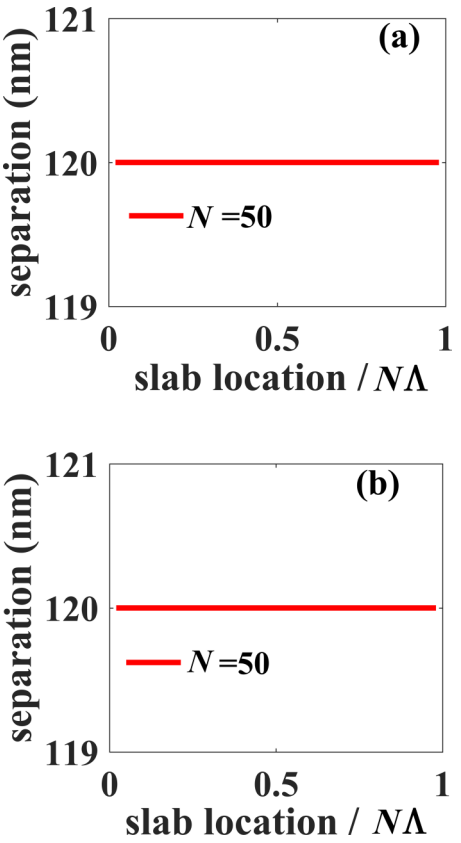

FIG. 5. The lattice constants of the PC illuminated by a pair of identical counterpropagating plane waves, which can be coherent (a) or incoherent (b).

phenomenon was observed in all simulations we performed. In fact, in all of our simulations, if the equilibrium configuration is a PC, one of its lower band edges always coincides with the incident wavelength. The more the slabs, the less deviation from the equilibrium configurations to the ideal PCs.

C. Stability analysis

We adopted the linear stability analysis from Ref. [21] to investigate the stability of the optically bound PC. In

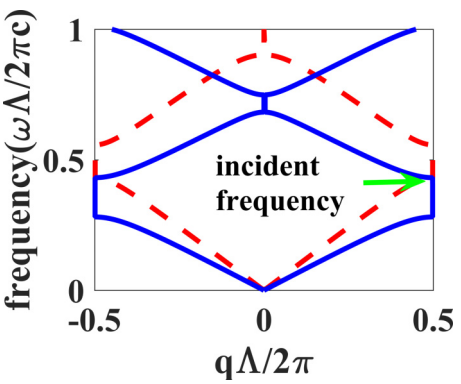

FIG. 6. Band structures of initial PC (solid blue line) and the newly formed PC (dashed red line). Clearly, the lower band edge of the final PC is aligned with the incident frequency.

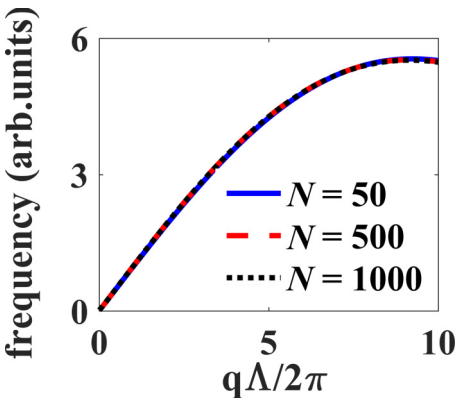

FIG. 7. Natural vibration frequencies for infinite PCs calculated by using the dynamical matrix approach, where the dynamical matrix is approximated by those of finite-sized PCs with 50 (solid blue line), 500 (dashed red line), and 1000 (dotted black line) slabs. The good agreement fors different N indicates good convergence. The frequencies are all positive, indicating stability.

short, their stabilities are dictated by the natural vibration frequencies through the dependence in $e^{-i\Omega t}$, where Ω is the natural vibration frequency. Depending on the nature of the natural vibration frequencies, the vibrational modes of an equilibrium configuration can be stable (real frequency), unstable (imaginary frequency), neutral (zero frequency), quasistable (complex frequency), or complex unstable (complex frequency) [21]. All periodic equilibrium configurations we found fulfill the condition that incident frequency matches one of the lower band edges of the PC. Moreover, all of them are stable in the sense that their natural vibration modes are real numbers.

We then considered the stability of an infinite PC by using the dynamical matrix approach which is outlined in the Appendix [34]. The needed dynamical matrix was calculated approximately by using the matrix formed by a finite PC with 50, 500, and 1000 slabs. The fact that the results for 50 (solid blue line), 500 (dashed red line), and 1000 (dotted black line) slabs agree excellently well with each other in Fig. 7 suggests a good convergence of our results. As shown in Fig. 7, the natural vibration frequencies are all real; it is clear that when a PC is illuminated at the lower band edge, we can find a stable equilibrium state even for an infinite PC. The existence of a stable PC when illuminated at the lower band edge can be understood heuristically [35]. The force is zero when both the arrangement of the slabs and the field patterns are symmetrical, which happens at the band edges only. In other frequencies, the slab arrangement is still symmetrical, but not the fields, so the force is not zero. At the lower band edge, the electromagnetic energy is mainly localized in the dielectrics; since the gradient force tends to drive dielectrics to the high-intensity region, the equilibrium is expected to be stable. On the contrary, for the upper band edge, even though it also corresponds to an equilibrium, its electromagnetic energy is localized in air, rendering it unstable.

D. One-dimensional PC with $\mathcal{PT}$ symmetry

Here, we consider a 1D PC system possessing $\mathcal{PT}$ symmetry. A one-dimensional $\mathcal{PT}$-symmetric PC is shown

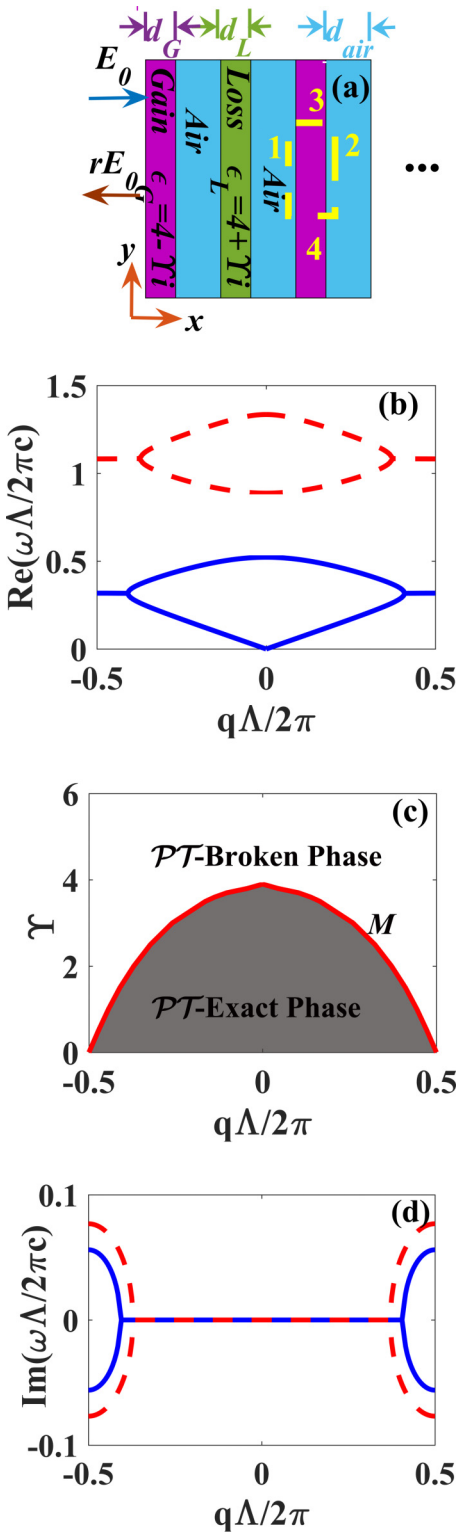

FIG. 8. (a) Schematic diagram showing a 1D $\mathcal{PT}$-symmetric PC. (b) Real part of the band structure for $\varepsilon_G = 4 - \Upsilon i$, $\varepsilon_L = 4 + \Upsilon i$, $\varepsilon_{\text{air}} = 1.0$, $\mu_G = \mu_L = \mu_{\text{air}} = 1$, $d_G = d_L = 80\,\text{nm}$, $d_{\text{air}} = 120\,\text{nm}$, and $\Upsilon = 2.0$. Here q is the Bloch wave vector, and the lattice constant is $\Lambda = d_G + d_L + 2d_{\text{air}}$. (c) Trajectories of the exceptional points of M in (q,Υ) space. The gray region stands for the $\mathcal{PT}$ exact phase, and the white region for the $\mathcal{PT}$ broken phase. (d) The imaginary part of the band structure for the same configuration in (b).

in Fig. 8(a) of which the real and imaginary parts of the band structure are plotted in Figs. 8(b) and 8(d) where $\varepsilon_G = 4 - \Upsilon i$, $\varepsilon_L = 4 + \Upsilon i$, $\varepsilon_{\text{air}} = 1.0$, $d_{\text{air}} = 120\,\text{nm}$ (thickness of the air), $d_G = d_L = 80\,\text{nm}$ (thickness of the dielectric with gain or loss), and $\Upsilon = 2.0$. The points where two lines in the band structure merge together are exceptional points [32,36–38] beyond which the band structure develops an imaginary component, corresponding to a broken $\mathcal{PT}$ symmetry. A nonzero positive imaginary part in the frequency implies the fields are unboundedly increasing with time ($\propto e^{-i\omega t} = e^{-i\text{Re}[\omega]t}e^{\text{Im}[\omega]t}$, it diverges with increasing t). Accordingly, the optical binding when the $\mathcal{PT}$ symmetry is broken will be more complicated and is a time-dependent problem. We shall not consider these situations here as they are not an equilibrium configuration. The trajectories of the exceptional points of M in the (q,Υ) space is plotted in Fig. 8(c). The gray region stands for the $\mathcal{PT}$ exact phase, while the white region stands for the $\mathcal{PT}$ broken phase. One can see that for $\Upsilon > 3.9$, there will be no $\mathcal{PT}$ exact phase for any q. For q and Υ within the $\mathcal{PT}$ exact phase region (shaded), the type of stable optical binding of PC we described in previous sections of this paper is possible.

Similar to a lossless PC, the lower band edge corresponds to a stable configuration. If we fixed the incident wavelength, Fig. 9(a) shows PCs with $\Upsilon = 2,4,5$ rearranged themselves into PCs with different lattice constants. However, in all cases, their lower band edges coincided with the incident wavelength [Fig. 9(b)]. Alternatively, in addition to having equilibrium configuration at the same wavelength, we can make the PCs with $\Upsilon = 2,4,5$ to share the same lattice constants. For each Υ, we chose the incident wavelength to match the lower band edge of the desired PC. The band structures of the PC after relaxation are plotted in Fig. 9(c), and their lattice constants at equilibriums are shown in Fig. 9(d), which are essentially the same for different Υ. Finally, the natural vibration frequencies for the $\mathcal{PT}$-symmetric PCs with 50, 500, and 1000 slabs were calculated and all of them are real and positive. This demonstrates that the equilibrium configurations are stable.

E. Oblique incidence

The lattice constants at equilibrium for 30°, 45°, 60°, and 80° are, respectively, 131.1 nm, 144.8 nm, 162.4 nm, and 182.9 nm. Initially the lower band edges associated with the four incident angles are at different frequencies; after relaxation, the PCs rearranged themselves such that all their lower band edges coincided with the incident wavelength. The stability is also verified by linear stability analysis.

III. CONCLUSION AND DISCUSSION

In the past two decades, researchers have tried to build large-scale optically bound "materials," but so far the effort has not been successful. Some believe the failure is due to the limited experimental setup such as the availability of laser power. Some suggests it is an intrinsic instability of the optical bound structure [2,39]. We demonstrated the optical binding of a stable periodic 1D structure, which is a photonic crystal illuminated at one of its lower band edges. We have repeated our calculations for PCs with different lattice constants and

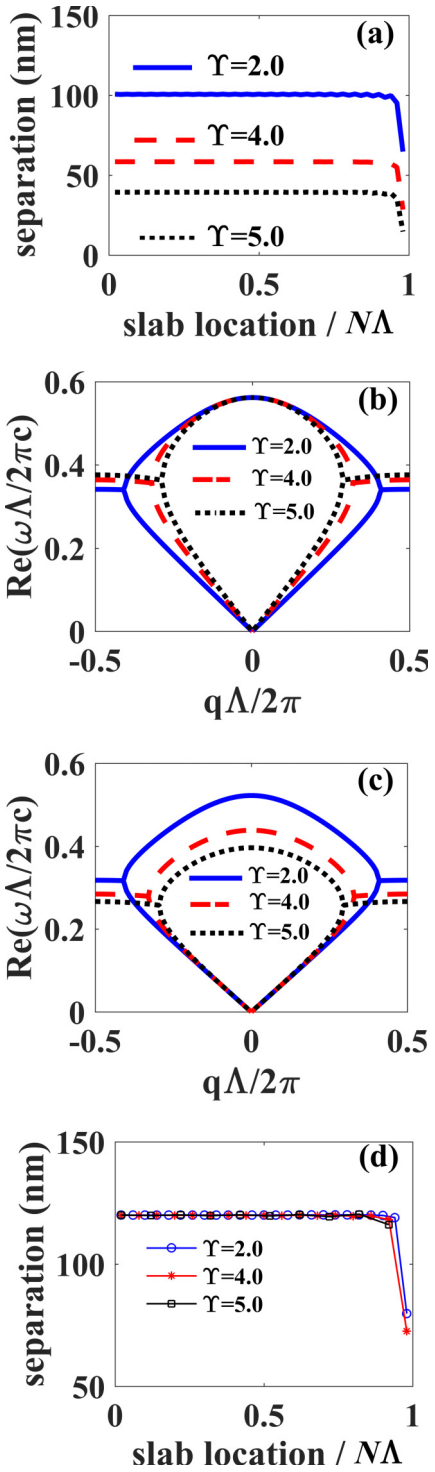

FIG. 9. (a) The separations between two adjacent slabs of the newly formed PCs ($N = 50$) with $\Upsilon = 2.0$ (solid blue line), $\Upsilon = 4.0$ (dashed red line), and $\Upsilon = 5.0$ (dotted black line). The incident frequency is 0.5625 ($\omega\Lambda/2\pi c$). (b) Band structure of the newly formed PCs with $\Upsilon = 2.0$ (solid blue line), $\Upsilon = 4.0$ (dashed red line), or $\Upsilon = 5.0$ (dotted black line). It is clear that the lower band edges of the newly formed PCs align with the incident frequency. (c) Band structure of the newly formed PCs with $\Upsilon = 2.0$ (solid blue line), $\Upsilon = 4.0$ (dashed red line), and $\Upsilon = 5.0$ (dotted black line). (d) The separations (lattice constants) between two adjacent slabs.

dielectric constants, and observed the same phenomenon. It appears to us that we can use our approach to build any PC with a single slab per unit cell, as long as the initial configurations are not too far away from it. For example, if we want to build a PC with a certain period, we can illuminate the collection of slabs with a laser with a frequency equal to that of the lower band edge of that desired PC. The collection of slabs will automatically relax to the appropriate positions.

By using the dynamical matrix approach, we showed a PC consisting of an infinite number of slabs can be stably bounded. Our detailed studies on optical force also allowed an additional degree of freedom in fine-tuning devices consisting of slabs, such as photonic crystals, superlattices, planar cavities, etc.

ACKNOWLEDGMENT

This work is supported by Hong Kong RGC through Grants No. HKBU 209913 and No. AoE/P-02/12.

APPENDIX

1. Dynamical matrix approach

We label the slabs with n and m; z_n denotes the z component of the equilibrium position of the nth slab and its displacement away from the equilibrium position is denoted by u_n. The optical force acting on slab m, F_m, which is a function of the coordinates of all slabs, can be expanded in a Taylor series about the equilibrium positions z_n:

$$F_m(z_n + u_n) = F_m(z_n) + \sum_{n,m} \frac{\partial F_m}{\partial u_n} u_n + \cdots$$
$$= F_m(z_n) + \sum_{n,m} F_n^m u_n + \cdots . \quad \text{(A1)}$$

For a static equilibrium, the first term is zero, because, by definition, there is no force at an equilibrium. For a dynamical equilibrium, F_m is independent of m by definition. As it is near the equilibrium, the linear term dominates. The higher terms in the expansion can be ignored.

The quantity $F_m^n u_m$ is thus the force exerted on slab n when slab m is displaced away from the equilibrium position by a distance u_m in the z direction.

2. Equation of motion

For the displacement u_n of slab n, Newton's law gives

$$M_n \ddot{u}_n - \sum_m F_m^n u_m = 0. \quad \text{(A2)}$$

For periodic structures, it is appropriate to write the displacement u_n in terms of a plane wave with respect to the slab coordinates according to the Bloch theorem:

$$u_n = \frac{1}{\sqrt{M_n}} u(q_z) e^{i(q_z z_n - \omega t)}. \quad \text{(A3)}$$

Here, q_z denotes the z component of the Bloch wave vector. Submitting this form into Eq. (A2) we can obtain an equation

for the amplitude u:

$$\omega^2 u(q_z) + \sum_m \frac{1}{\sqrt{M_n M_m}} F_m^n e^{iq_z(z_m - z_n)} u(q_z) = 0. \quad \text{(A4)}$$

Let

$$D_m^n(q_z) = -\frac{1}{\sqrt{M_n M_m}} F_m^n e^{iq_z(z_m - z_n)}. \quad \text{(A5)}$$

Here, $D_m^n(q_z)$ is the component of the dynamical matrix $\overleftrightarrow{\boldsymbol{D}}(q_z)$. A system of linear homogeneous equations only has solutions (eigensolutions) when the following determinant vanishes:

$$\mathrm{Det}\{\overleftrightarrow{\boldsymbol{D}}(q_z) - \omega^2 \overleftrightarrow{\boldsymbol{I}}\} = 0. \quad \text{(A6)}$$

Here $\overleftrightarrow{\boldsymbol{I}}$ is the identity matrix.

The dynamical matrix needed is approximated by using the matrix formed by a finite PC with 50, 500, and 1000 slabs, and the resultant natural vibration frequencies are plotted in Fig. 6. The fact that the results for 50, 500, and 1000 slabs possess excellent agreement with each other indicates the convergence of our results. As the natural vibration frequencies are all positive, it is clear that even for an infinite PC, at the lower band edge, we can find a stable equilibrium state.

[1] A. Ashkin, *Optical Trapping and Manipulation of Neutral Particles Using Lasers* (World Scientific, Singapore, 2006).
[2] G. Grier, Nature **424**, 810 (2003).
[3] K. Dholakia and P. Reece, Nano Today **1**, 18 (2006).
[4] K. Dholakia, P. Reece, and M. Gu, Chem. Soc. Rev. **37**, 42 (2008).
[5] F. M. Fazal and S. M. Block, Nat. Photonics **5**, 318 (2011).
[6] K. Dholakia and T. Cizmar, Nat. Photonics **5**, 335 (2011).
[7] M. Padgett and R. Bowman, Nat. Photonics **5**, 343 (2011).
[8] M. M. Burns, J. M. Fournier, and J. A. Golovchenko, Phys. Rev. Lett. **63**, 1233 (1989).
[9] M. I. Antonoyiannakis and J. B. Pendry, Europhys. Lett. **40**, 613 (1997).
[10] M. I. Antonoyiannakis and J. B. Pendry, Phys. Rev. B **60**, 2363 (1999).
[11] K. Dholakia and P. Zemanek, Rev. Mod. Phys. **82**, 1767 (2010).
[12] M. M. Burns, J. M. Fournier, and J. A. Golovchenko, Science **249**, 749 (1990).
[13] S. A. Tatarkova, A. E. Carruthers, and K. Dholakia, Phys. Rev. Lett. **89**, 283901 (2002).
[14] W. Singer, M. Frick, S. Bernet, and M. Ritsch-Marte, J. Opt. Soc. Am. B **20**, 1568 (2003).
[15] C. D. Mellor and C. D. Bain, ChemPhysChem **7**, 329 (2006).
[16] C. D. Mellor, T. A. Fennerty, and C. D. Bain, Opt. Express **14**, 10079 (2006).
[17] V. Karasek, K. Dholakia, and P. Zemanek, Appl. Phys. B: Lasers Opt. **84**, 149 (2006).
[18] N. K. Metzger, K. Dholakia, and E. M. Wright, Phys. Rev. Lett. **96**, 068102 (2006).
[19] V. Karasek, T. Cizmar, O. Brzobohaty, P. Zemanek, V. Garces-Chavez, and K. Dholakia, Phys. Rev. Lett. **101**, 143601 (2008).
[20] O. Brzobohaty, T. Cizmar, V. Karasek, M. Siler, K. Dholakia, and P. Zemanek, Opt. Express **18**, 25389 (2010).
[21] J. Ng, Z. F. Lin, C. T. Chan, and P. Sheng, Phys. Rev. B **72**, 085130 (2005).
[22] P. C. Chaumet and M. Nieto-Vesperinas, Phys. Rev. B **64**, 035422 (2001).
[23] F. Depasse and J. M. Vigoureux, J. Phys. D: Appl. Phys. **27**, 914 (1994).
[24] S. K. Mohanty, J. T. Andrews, and P. K. Gupta, Opt. Express **12**, 2746 (2004).
[25] J. M. Taylor and G. D. Love, Opt. Express **17**, 15381 (2009).
[26] J. M. Taylor, *Optical Binding Phenomena: Observations and Mechanisms* (Springer, Berlin, 2011).
[27] M. C. Frawley, I. Gusachenko, V. G. Truong, M. Sergides, and S. Nic Chormaic, Opt. Express **22**, 16322 (2014).
[28] M. Guillon, O. Moine, and B. Stout, Phys. Rev. Lett. **96**, 143902 (2006).
[29] X. Han and P. H. Jones, Opt. Lett. **40**, 4042 (2015).
[30] A. Yariv and P. Yeh, *Optical Waves in Crystals: Propagation and Control of Laser Radiation* (Wiley, New York, 1984).
[31] J. Israelachvili, *Intermolecular and Surface Force*, 2nd ed. (Academic Press, London, 1991).
[32] C. E. Rüter, K. G. Makris, R. E. Ganainy *et al.*, Nat. Phys. **6**, 192 (2010).
[33] J. D. Jackson, *Classical Electrodynamics*, 3rd ed. (John Wiley & Sons, New York, 1999), p. 261.
[34] H. Ibach and H. Lüth, *Solid State Physics* (Springer, Berlin, 1993).
[35] J. D. Joannopoulos, S. G. Johnson, J. N. Winn, and R. D. Meade, *Photonic Crystal: Molding the Flow of Light*, 2nd ed. (Princeton University Press, Princeton, NJ, 2008).
[36] A. Mostafazadeh, Phys. Rev. Lett. **102**, 220402 (2009).
[37] C. Z. Shi, M. Dubois, Y. Chen, L. Cheng, H. Ramezani, Y. Wang, and X. Zhang, Nat. Commun. **7**, 11110 (2016).
[38] L. Ge, Phys. Rev. X **4**, 031011 (2014).
[39] Z. H. Hang, J. Ng, and C. T. Chan, Phys. Rev. A **77**, 063838 (2008).